On Impact and Volcanism across the Cretaceous-Paleogene Boundary

Pincelli M. Hull[1*♦], André Bornemann[2*♦], Donald Penman[1♦], Michael J. Henehan[1,3♦], Richard D. Norris[4♦†], Paul A. Wilson[5♦†], Peter Blum[6♦†], Laia Alegret[7], Sietske Batenburg[8†], Paul R. Bown[9†], Timothy J. Bralower[10], Cecile Cournede[11,12†], Alexander Deutsch[13†], Barbara Donner[14], Oliver Friedrich[15†], Sofie Jehle[16†], Hojung Kim[9†], Dick Kroon[17], Peter Lippert[18†],Dominik Loroch[13†], Iris Moebius[15,19†], Kazuyoshi Moriya[20†], Daniel J. Peppe[21], Gregory E. Ravizza[22†], Ursula Röhl[14†], Jonathan D. Schueth[23], Julio Sepúlveda[24†], Philip Sexton[25†], Elizabeth Sibert[4,26,27†], Kasia K. Śliwińska[28†], Roger E. Summons[29†], Ellen Thomas[1,30], Thomas Westerhold[14†], Jessica H. Whiteside[5†], Tatsuhiko Yamaguchi[31†], James C. Zachos[32]

[1] Department of Geology and Geophysics, Yale University, 210 Whitney Ave, New Haven, CT 06511, USA
[2] Bundesanstalt für Geowissenschaften und Rohstoffe, Stilleweg 2, 30655 Hannover, Germany
[3] GFZ German Research Centre for Geosciences, Telegrafenberg, 14473 Potsdam, Germany
[4] Scripps Institution of Oceanography, University of California San Diego, 9500 Gilman Drive, La Jolla, CA 92093-0244, USA
[5] National Oceanography Centre Southampton, University of Southampton, Waterfront Campus, European Way, Southampton SO14 3ZH, UK
[6] International Ocean Discovery Program, Texas A&M University, 1000 Discovery Drive, College Station, TX 77845, USA
[7] Departamento de Ciencias de la Tierra & Instituto Universitario de Ciencias Ambientales, Universidad Zaragoza, 50009 Zaragoza, Spain
[8] Géosciences, Université de Rennes 1, Campus de Beaulieu, 35042 Rennes, France
[9] Department of Earth Sciences, University College London, Gower Street, London WC1E 6BT, UK
[10] Department of Geosciences, Pennsylvania State University, University Park, PA, USA
[11] CEREGE, Université Aix-Marseille, Europole de l'Arbois BP 80 1, 13545 Aix en Provence, France
[12] Institute for Rock Magnetism, University of Minnesota, John T. Tale Hall, 116 Church St. SE, Minneapolis, MN 55455, USA
[13] Institut für Planetologie, Universität Münster, Wihelm-Klemm-St. 10, 48149 Münster, Germany
[14] MARUM – Center for Marine Environmental Sciences, University of Bremen, Leobener Strasse 8, 28359 Bremen, Germany
[15] Institute of Earth Sciences, Heidelberg University, Im Neuenheimer Feld 234-236, 69120 Heidelberg, Germany
[16] Institut für Geophysik und Geologie, Universität Leipzig, Talstr. 35, 04103 Leipzig, Germany
[17] School of Geosciences, University of Edinburgh, Edinburgh EH8 9XP, United Kingdom
[18] Department of Geology & Geophysics, The University of Utah, 115 S 1460 E, Salt Lake City, UT 84112-0102, USA
[19] Department of Biogeochemical Systems, Max Planck Institute for Biogeochemistry, Hans-Knöll St. 10, 07745 Jena, Germany
[20] Department of Earth Sciences, Waseda University, Nishiwaseda 1-6-1, Shinjyuku-ku, Tokyo 169-8050, Japan
[21] Department of Geosciences, Baylor University, One Bear Place #97354, Waco Texas 76798-7354, USA
[22] Department of Geology & Geophysics, University of Hawai'I at Manoa, Honolulu, HI 96822, USA
[23] ConocoPhillips Company, 925 N Eldridge Pkwy, Houston, TX 77079, USA
[24] Department of Geological Sciences and Institute of Arctic and Alpine Research, University of Colorado Boulder, UCB 450, Boulder CO 830309-0450, USA
[25] School of Environment, Earth & Ecosystem Sciences, The Open University, Walton Hall, Milton Keynes MK7 6AA, UK
[26] Harvard Society of Fellows, Harvard University, 78 Mount Auburn Street, Cambridge, MA 02138, USA
[27] Department of Earth and Planetary Sciences, Harvard University, 20 Oxford Street, Cambridge, MA 02138, USA
[28] Department of Stratigraphy, Geological Survey of Denmark and Greenland (GEUS), Øster Voldgade 10, DK-1350 Copenhagen K, Denmark
[29] Department of Earth, Atmospheric and Planetary Science, Massachusetts Institute of Technology, Cambridge, MA 02139, USA
[30] Department of Earth and Environmental Sciences, Wesleyan University, Middletown CT 06459, USA
[31] National Museum of Nature and Science, 4-1-1 Amakubo, Tsukuba, 305-0005, Japan
[32] Department of Earth and Planetary Sciences, University of California Santa Cruz, CA 95064, USA

[*] Co-first authors (pincelli.hull@yale.edu and andre.bornemann@bgr.de)
[♦] First seven authors in order of contribution, all others alphabetical
[†] Primary Contribution: IODP Expedition 342 K/Pg boundary investigation

Abstract

The cause of the end-Cretaceous mass extinction is vigorously debated due to the occurrence of a very large bolide impact and flood basalt volcanism near the boundary. Disentangling their relative importance is complicated by uncertainty regarding kill mechanisms and the relative timing of volcanogenic outgassing, impact, and extinction. We use carbon cycle modeling and paleotemperature records to constrain the timing of volcanogenic outgassing. We found support for major outgassing beginning and ending distinctly prior to the impact, with only impact coinciding with mass extinction and biologically amplified carbon cycle change. Our models show that these extinction-related carbon cycle changes would have allowed the ocean to absorb massive amounts of CO_2, thus limiting the global warming otherwise expected from post-extinction volcanism.

Introduction

Sixty-six million years ago two planetary-scale disturbances occurred within less than a million years of one another. An asteroid of more than 10 km in diameter collided with the Yucatan Peninsula at the boundary between the Cretaceous and the Paleogene (~66 Ma), producing the ~200 km wide Chicxulub impact crater (*1-4*). Impact markers at hundreds of sites globally co-occur with the deposition of the Cretaceous-Paleogene (K/Pg) boundary clay and include elevated abundances of siderophilic elements such as iridium, osmium, and nickel, and tektites and shocked quartz (*1, 5, 6*). During the K/Pg boundary-spanning magnetochron C29r (65.688-66.398 Ma, ~ 710,000 years long (*7*)), an estimated ~500,000 km^3 of lava flooded across much of India and into the deep sea in a large igneous province (LIP) known as the Deccan Traps (*8, 9*). Deccan volcanism was, like most flood basalt eruptions (*9-11*), episodic, with flows deposited in pulses throughout magnetochron C29r (*12, 13*). That both volcanism and the impact event occurred within several hundred thousand years of the K/Pg extinctions is beyond reasonable doubt (*5, 9, 12, 13*). However, this still leaves many aspects uncertain, including the relative timing and magnitude of volcanic effects on the biosphere (*13, 14*), the potential relationship between impact and volcanism (*8, 13, 15*), and whether impact or volcanism acted as the sole, primary, or joint drivers of extinction (*5, 10, 16*).

The case for the Chicxulub impact as a driver of K/Pg mass extinction includes processes hypothesized to operate during the days and decades following the collision. The bolide impact injected an estimated >50,000 km^3 of ejecta (*4*), ~ 325 Gt of sulfur and ~425 Gt CO_2 and other volatiles (*17*) into the atmosphere from the marine carbonate and anhydrite target rock of the Yucatan Peninsula (*5, 18*). The combined effects of an expanding impact fireball and the re-entry of molten ejecta from the skies (*19*) may have raised temperatures to the point of spontaneous combustion near the impactor and caused severe heat stress and even death many thousands of km away from the impact site in minutes to days after impact (*20*). In the days to years that followed, nitrogen and sulfur vapors reacted to form nitric and sulfuric acids and, with CO_2 gases, acidified the oceans (*21-23*). Finally, models and empirical evidence suggest that the combination of dust and aerosols precipitated a severe impact winter in the decades post-impact (*24-27*).

Impressive though these environmental effects may be, some researchers question whether the Chicxulub impactor acted as the sole or main driver of the K/Pg mass extinction for three primary reasons. First, no single kill mechanism appears to explain the extinction patterns: acidification (*28, 29*) and primary productivity decline (*30*) (due to darkness and cold (*26*)) are favored in the marine realm, whereas heat exposure and/loss of productivity (due to fires, darkness and cold (*18, 26*)) are favored in the terrestrial realm (*31, 32*). Second, asteroid and comet impacts occur throughout the history of life (although likely none in the last ~500 Myr of the size and force of Chicxulub (*33*)), but no other mass extinction is unambiguously linked to such a collision (*34*). Third, flood basalt volcanism is strongly implicated as the driver of two of the greatest mass extinctions in the last half billion years (the Permian-Triassic [P/T] and Triassic-Jurassic [T/J]) leading some to favor a similar role for Deccan volcanism in the K/Pg mass extinction (e.g., *35*). However, most episodes of flood basalt volcanism after the T/J produced no increase in extinction rates (*36*), potentially due to important Earth system changes that dampened the effects of flood basalts post-P/T.

Questions regarding the role of Deccan volcanism in driving the K/Pg mass extinction arise because of the relative lack of evidence for a volcanogenic driver. Despite advances in chronology, the timing of the most voluminous Deccan eruptions relative to the K/Pg extinctions remains unclear (e.g., ref. 8 vs. 9). Many earlier authors argued that most Deccan flood basalts (>85%) were emplaced in a relatively short interval before the K/Pg, starting around the C29r/C30n boundary (~66.39 Ma) and ending well before the K/Pg impact (*11, 12*). In contrast, Renne et al. (*13*) and Sprain et al. (*9*) proposed that the vast majority of Deccan basalts were emplaced after the impact. Schoene et al. (*8*) largely agree with the basalt flow ages of refs. 9 and 13, but place the K/Pg boundary higher in the lava pile (i.e., the upper part of, or above, the Poladpur unit), and therefore propose major pulses of emplacement just before and just after the impact (*8*).

Pre- and post-impact scenarios are debated in part because they are tied to different environmental disruption scenarios. Pre-event volcanism may have acted in concert with the impact to drive K/Pg extinctions (*10*), whereas post-event volcanism suggests a role for volcanism in the delayed recovery of biodiversity (*13*). For the environment and life, the main environmental effects of large igneous provinces are attributed to volatile release (*37-39*), not lava emplacement, and the magnitude of volcanic outgassing is not necessarily linked directly to the volume of erupted lava. If early eruptive phases of flood basalt volcanism have higher volatile concentrations, then most volatiles could have been released before the impact, even if most of the lava was emplaced afterwards (*9*).

Here we provide constraints on Deccan Trap outgassing by comparing exceptionally well-resolved and temporally detailed ocean drilling and global temperature records, with five modeled end-member scenarios for the timing, magnitude, and composition of outgassing (*40*). These comparisons allow us to consider the relative effects of Deccan Trap outgassing and bolide impact on the marine carbon cycle and biological change.

Marine environmental record of outgassing

Deccan Trap degassing released a mix of volatiles including sulfur dioxide (SO_2), chlorine (Cl) and other halogens, and carbon dioxide (CO_2), with sulfur having perhaps the greatest direct effect on ecosystems through acidification and pronounced global cooling (>4.5°C) (*38*). The environmental effects of sulfur dioxide, however, would have been relatively short-lived (years to centuries at most) and difficult to detect in slowly accumulating deep-sea sediments. In contrast, the influence of CO_2 emissions should be clearly evident in marine sediments as a global warming event paired with a carbon isotope anomaly (*41*). We used this diagnostic fingerprint of CO_2 emissions as a proxy for the timing of potentially disruptive outgassing of sulfur (and other noxious gasses) and to test which volcanic degassing scenarios are compatible with the observed record.

Two dominant features are clear in our global temperature compilation (Fig. 1) (*40*). First, marine and terrestrial records show a late Maastrichtian warming event of ~2°C on average (Figs. S1-S16; *42, 43, 44*) in the Cretaceous part of C29r that cools back to pre-event temperatures prior to the K/Pg boundary (Fig. 1). Second, the earliest Danian has temperatures comparable to those in the late Maastrichtian prior to the warming event, with temperatures gradually increasing to become >1°C warmer on average by ~600 kyr after the impact. Benthic foraminiferal oxygen isotope records typically track changes in global mean temperatures, and they show both these features (Figs. 1, 2, S13a), as do most other archives (Figs. S1-S16). The two exceptions are the bulk carbonate records and fish teeth phosphate records from El Kef (Figs. S10c, S11, S12), which likely do not track global temperature for extinction-related reasons (*40*), thus we excluded them from the calculation of global mean temperatures.

Our multiproxy, astronomically tuned record from the North Atlantic site (*45*) has an exceptionally complete Maastrichtian sequence and a mm-thick tektite layer at the K-Pg boundary (Figs. 2, S17-S19). The record documents an excursion to lower values in $\delta^{13}C$ in bulk sediments coincident with $\delta^{18}O$ decline (a warming indicator) as well as a decline in osmium isotope values (Fig. 2, S20-S21). Similar patterns are seen in records from the South Atlantic Walvis Ridge and the North Pacific Shatsky Rise (Figs. 2, S18-S19; *42, 46*). The similarity of these records amongst three such widespread localities and four sites (Fig. 2), suggests that they provide a remarkably complete record of magnetochron C29r. Slight temporal offsets in the apparent onset and recovery from latest Maastrichtian warming (among all sites) and in early Paleogene carbon isotope patterns at Shatsky Rise, due either to short unconformities and/or the limitations of cyclostratigraphic age models, illustrate the current temporal uncertainties (Fig. 2). Temperature and atmospheric CO_2, as reflected in both our $\delta^{18}O$ and $\delta^{13}C$ anomalies, and recent boron isotope records (*23*), returned to pre-warming values in the very latest Maastrichtian. The most prominent feature in the records is the dramatic decline in $\delta^{13}C$ isotopes and change in sedimentary $CaCO_3$ content beginning at the K/Pg boundary (Fig. 2).

We investigated the timing of Deccan Trap outgassing by modeling the effects of CO_2 and sulfur emissions on long-term global temperatures using the geochemical box model LOSCAR (Long-term Ocean Sediment CArbon Reservoir v. 2.0.4) (*47*). Guided by published hypotheses for the timing and volume of trap emplacement, we tested five major Deccan Trap emission scenarios differing in the timing of volatile release: (i) Case 1: Leading, majority (87%) of degassing pre-K/Pg boundary (after (*10*)) (ii) Case 2: 50/50, half of degassing prior to and half following the K/Pg boundary (after lower estimate in (*9*)); (iii) Case 3: Punctuated, four pulses with one major event just preceding the K/Pg boundary (after (*8*)), (iv) Case 4: Lagging, majority (87%) of degassing post-K/Pg boundary (inverse Case 1 pre-/post- outgassing volumes, (*13*)); and (v) Case 5: Spanning, emissions released evenly throughout magnetochron C29r (after (*12*)) (Table 1). All volcanic outgassing scenarios assume the same (i) initial climatic and oceanographic conditions: 600 ppm pCO_2 and climate sensitivity of 2-4°C per CO_2 doubling (*41*), LOSCAR's Paleogene ocean configuration and circulation, and marine [Mg^{2+}] of 42 mmol/kg and [Ca^{2+}] of 21 mmol/kg; (ii) K/Pg impact volatile release from the target rock (325 Gt S; 425 Gt CO_2)(*17*); (iii) upper and lower end-estimates for total volcanic outgassing volumes (4091-9545 Gt C and 3200-8500 Gt S (*10*) at constant ratios) (*40*); and iv) extinction related changes in the marine carbon cycle (*41, 48*) (including reductions in both organic carbon and carbonate export and increases in intermediate-depth organic carbon remineralization, see Table 1) that taper back to pre-event values over 1.77 Myr following the extinction (*49*). In most outgassing scenarios, we assumed a common onset of Deccan degassing at the C30n/C29r boundary, following geochronology of the traps (*8, 9, 12, 50*). In the GTS 2012 age framework (*7*) used to align the temperature records, C30n/C29r is 358 kyr prior to the K/Pg boundary, rather than the ~250-300 kyrs indicated by the most recent $^{40}Ar/^{39}Ar$ and U-Pb geochronology (*8, 50*). Simulations were initially tuned (*40*) to find the biological scenario (iv) that minimized data-model mismatches (Figs. S22-S27) and multiple scenarios for climate sensitivity and outgassing are considered in assessing goodness of fit (Figs. 3-4, S25, S28-S32, Table 2).

Three modeled scenarios differ distinctly from the observed pattern of temperature change (Fig. 3), thus we consider them unlikely to represent the true outgassing history. Case 3 fails to reproduce the late Maastrichtian warming and shows a pronounced boundary-crossing warming event that is not supported by proxy data. In Case 4, late Maastrichtian warming is too muted and early Paleocene warming is too pronounced, and in Case 5 warming increases up to the K/Pg boundary, unlike the empirical record (Fig. 3). Relatively poor model fit is also indicated by high mean absolute errors (MAEs) for Cases 3 and 4 as compared to Cases 1 and 2 (Table 2). The temporal dynamics of $\delta^{13}C$ in Cases 3 and 5 also deviate from the empirical record (Fig 4).

Only two outgassing scenarios produce modeled temperatures resembling the empirical records: the leading case (Case 1) and the 50:50 case (Case 2). We thus consider these the two most likely of the tested scenarios to represent Deccan Trap outgassing. In Case 1, most CO_2 and SO_2 degassing occurred in the latest Maastrichtian, leading to global warming and subsequent cooling prior to the K/Pg. The relatively constant early Paleocene temperatures of Case 1, with a gradual warming over the 600kyrs following the impact, are also consistent with empirical records (Figs. 1-3, S17-S18). Case 2 (50:50) also matches the empirical temperature record well (Fig. 3), with the lowest MAEs of all cases (Table 2). The Late Cretaceous warming differs between Case 1 and Case 2 due to the reduced Late Cretaceous volcanic outgassing in the latter. Although uncertainty about climate sensitivity (*51*) and total Deccan Trap emissions (*10, 12*) has a greater effect on modeled temperatures than the difference in outgassing volume (Figs. 3, S25, S28), carbon isotopes also support Case 2 as the more likely scenario (Fig. 4; MAEs in Table S31).

The climatic effects of a major pulse (50%) of Deccan outgassing released over the ~350 kyr immediately following the impact (Case 2) were limited by extinction-related changes to the carbon cycle, including the reduction in $CaCO_3$ export from pelagic calcifiers to the seafloor. Marine $CaCO_3$ export indirectly affects atmospheric CO_2 by changing the distribution of carbon and alkalinity between the surface and deep-ocean, and slows the removal of alkalinity from the system via $CaCO_3$ burial (*41*). The difference between Case 1 and 2 is almost imperceptible, with Case 2 having slightly warmer (~0.25°C) early Danian temperatures than Case 1. Notably, more rapid Paleocene outgassing, such as modeled in Case 3 (ref. 8), exceeds the capacity of the altered marine carbon cycle to absorb CO_2.

Our results inform several important boundary debates. First, if there was a large pulse of emplacement just 20-60 kyrs prior to the impact (*8*), most CO_2 outgassing (and associated environmental impacts) must have preceded lava emplacement by several hundred thousand years. This would be prior to the eruption of the most voluminous stages of Deccan volcanism (i.e., pre-Wai subgroup) as modeled for Case 1 and 2 (Fig. 3-4; see expanded discussion in (*40*)). Second, roughly equal pre- and post-impact volcanic degassing is supported (i.e., Case 2, Figs. 3-4), a hypothesized scenario in ref. 9. However, our results are not consistent with most (>75%) volcanogenic degassing post-impact (i.e., outgassing more similar to eruptive volumes in refs. *9, 13*), because modeled warming is too muted in the Cretaceous and too pronounced in the early Paleocene (i.e., Case 4) as compared to empirical records (Fig. 3). Third, impact-related volatile release from the target rock has a negligible climatic effect (Fig. S24), so is unlikely to account for the dramatic warming indicated by fish teeth $\delta^{18}O$ in the first 100 kyr (*52*). Instead, this record likely predominantly reflects changes in fish biology rather than temperature. Fourth, biotic recovery can account for the apparently gradual early Danian warming as observed in marine records if it begins at or shortly after impact and occurs over >1.5 myr. This biotic recovery scenario reproduces the general pattern of change in $\delta^{13}C$ gradients (Figs. 2, S27), carbonate saturation state (Figs. 2c, S27) and temperature, but differs from recovery hypotheses that posit a delay in the onset of biological recovery for ~ 500kyr or more (e.g., *40, 49, 53*).

No marine evidence for joint cause in mass extinction

The fossil record indicates no lasting, outsized, or cascading effect of the late Maastrichtian warming event on marine ecosystems of the sort that might predispose them to mass extinction by impact. First, we found no evidence for elevated extinction rates in the latest Cretaceous in marine taxa (Table S1), excepting a contested record from Seymour Island, Antarctica (e.g., *54, 55*). The scarcity of biostratigraphic datums in the Cretaceous portion of magnetochron C29r signifies a conspicuous lack of extinction in widespread species including planktonic foraminifera, nannoplankton, radiolarians, and ammonites (*7*). Second, late Cretaceous outgassing did not have a lasting effect on the community structure of well-fossilized taxa. Although range and community shifts coincided with warming, a shift back to the pre-warming-like communities occurred prior to impact (see Table S1). Third, marine carbon cycle indicators

($\delta^{13}C$ and carbonate deposition) show no discernable effect of late Maastrichtian outgassing and warming on a major ecosystem function: the export and cycling of carbon. The $\delta^{13}C$ anomaly size (~0.2-0.3 per mil; see also ref. *44*) is consistent with a volcanogenic driver as in Case 2 (Figs. 2, 4, S28) given the magnitude of warming, without biological amplification.

In contrast, major and enduring changes to ecosystems coincided with the K/Pg impact. In deep-sea records, impact markers occur at the level of the abrupt mass extinction of >90% planktonic foraminifera and 93% of nannoplankton species (Fig. 2). These groups exhibit rapid turnover and high dominance in community composition in the first 500 kyrs of the Paleocene (*56, 57*), an interval where bulk carbonate $\delta^{18}O$ likely reflects community composition rather than surface ocean temperatures (Figs. 5, S33-S35). At the same time, tracers of the marine carbon cycle indicate a profound change in marine ecosystem function. The community structure of some groups such as small fishes, which show no evidence of elevated extinction, changed permanently (*58*). The $\delta^{13}C$ composition of planktonic foraminifera and nannoplankton fell to or below that of benthic foraminifera at the iridium anomaly (Figs. 2,5, S34-S35; *43, 49*). The loss or inversion of the $\delta^{13}C$ gradient typically maintained by the biological pump is unmatched in the fossil record of pelagic calcifiers (~170 million years), and indicates that the K/Pg boundary impact had an outsized effect on the marine carbon cycle.

After the impact, an already altered marine carbon cycle is needed to counteract the CO_2 emitted by a major post-impact pulse of outgassing as in Case 2 (Fig. 3) to avoid a warming event of the same magnitude as the Late Cretaceous warming event. This suggests that the major ecological change of the K/Pg mass extinction must have occurred prior to any major post-impact volcanism. Our modeling does support a scenario in which Deccan volcanism could have contributed to the aftermath of the impact and mass extinction as in (*13*), if environmentally destructive gases such as SO_2, halogens, or sulfate aerosols contributed to (or drove) the persistence of unusual marine communities for the first ~500 kyrs of the Paleocene. This might be particularly true if the evolution of the magma chamber led to higher sulfur content of later emissions, as in other eruption types (*59*). However, no observations document acidification coupled to extreme cold snaps in the earliest Paleocene as predicted by this hypothesis, and there is no explanation for why SO_2 would have greater biotic effects in the well-buffered early Danian oceans than in the latest Maastrichtian oceans (Fig. S1-S18).

Conclusion

We combined climatic, biotic, and carbon cycle records with modeled impact and outgassing scenarios, and found support for a bolide impact as the primary driver of the end-Cretaceous mass extinction. Our analysis suggests that roughly 50% of Deccan Trap CO_2 outgassing occurred well before the impact, but does not support the suggestion (*8*) that a large outgassing event took place just before (~10-60 kyrs). This suggests a pronounced decoupling between CO_2 outgassing and lava flow emplacement if ref. 8 is correct, or a relative impact and eruption chronology similar to ref. 9 and our best-supported, 50:50 outgassing scenario. The Late Cretaceous warming event attributed to Deccan degassing is of a comparable size to small warming events in the Paleocene and early Eocene that are not associated with elevated extinction or turnover (*43, 60*), similar to what we find for the late Maastrichtian. We therefore conclude that impact and extinction created the initial opportunity for the rise of Cenozoic species and communities, but Deccan volcanism might have contributed to shaping them during the extinction aftermath.

Acknowledgements: This research used samples and/or data provided by the International Ocean Discovery Program (IODP), which was sponsored by the US National Science Foundation and participating countries under management of Joint Oceanographic Institutions, Inc, and its predecessors –the (Integrated) Ocean Drilling Program and the Deep Sea Drilling Program. We thank the JOIDES Resolution crew of IODP Expedition 342 and W. Hale and A. Wuelbers for help with sampling. We also thank the many centers and staff scientists who enabled the measurements, including Leanne Elder in the Hull Lab (Yale University), Brad Erkkila and Marvin Wint at the Yale Analytical and Stable Isotope Center, Dyke Andreasen at the UCSC Stable Isotope Laboratory, and F. Demory (CERGE) for help with magnetic data production and processing. This work benefited from helpful discussions with Jaume Dinarès-Turell, the insights of C. Brenhin Keller, and the comments of four anonymous reviewers.

Funding: IODP USSSP Post-Expedition Activity award and Yale University support to P.M.H.; Deutsche Forschungsgemeinschaft [DFG; grant numbers BO2505/8-1, EH 89/20-2] funding for

A.B.; Yale Peabody Museum support to M.J.H.; Spanish Ministry of Economy and Competitiveness and FEDER funds (CGL2017-84693-R) to L.A.; DFG funding [grant number VO687/14] to S.J.B.; a Richard Foster Flint Postdoctoral Fellowship (Dept. G&G, Yale University) for D.P.; DFG funding [grant number FR2544/2] to O.F.; NSF funding (EAR-132552) and American Chemical Society Petroleum Research Fund grant (PRF#52822-DN18) to D.J.P; DFG funding [grant numbers RO1113/3, RO1113/4, and RO1113/8] to U.R.; a NASA Exobiology Program grant (NNX09AM88G) to R.E.S.; a Danish Council for Independent Research/Natural Sciences (DFF/FNU; Grant 11-107497) award to K.K.Ś; NSF funding (OCE #1536611) to E.T; DFG funding [grant number WE5479/3] to T.W; and a NERC (NE/K006800/1) and Royal Society Wolfson award to P.A.W. **Author contributions:** Among the first six authors, P.M.H conceived and co-led the study, drafted the manuscript, contributed to model design, generated empirical data, and edited data tables and figures; A.B. co-led the study and coordinated data generation, reporting, figures, and tables, generated empirical data and substantially contributed to the study design and text; D.P. led LOSCAR modeling and substantially contributed to study design and text, M.J.H. compiled and aligned age models for the global temperature compilation, prepared related tables and figures, and substantially contributed to the study design and text; R.D.N., P.A.W, and P.B. led IODP Expedition 342, with R.D.N. and P.A.W. substantially contributing to study design and text. Among the remaining co-authors, L.A., S.B., P.R.B., T.J.B., C.C., A.D., B.D., O.F., S.J., H.K., D.K., P.L., D.L., I.M., K.M., D.J.P., G.E.R., U.R., J.S., J.D.S., E.S., K.K.Ś., R.E.S., E.T., T.W., J.H.W., and T.Y. contributed empirical datasets, figures, and related analyses, interpretations and text; and L.A., P.R.B., T.J.B., O.F., D.K., P.S., J.S., E.T., T.W., J.H.W., J.C.Z. substantially contributed to ideas and/or text. All authors read and approved the final text. **Data and materials availability:** all data is available in the manuscript and the supplementary material.

References

1. L. W. Alvarez, W. Alvarez, F. Asaro, H. V. Michel, Extraterrestrial cause for the Cretaceous-Tertiary extinction - experimental results and theoretical interpretation. *Science* **208**, 1095-1108 (1980).
2. A. R. Hildebrand *et al.*, Chicxulub crater - a possible Cretaceous Tertiary Boundary impact crater on the Yucatan Peninsula, Mexico. *Geology* **19**, 867-871 (1991).
3. B. Collen *et al.*, Clarifying misconceptions of extinction risk assessment with the IUCN Red List. *Biology Letters* **12**, 20150843 (2016).
4. J. Morgan *et al.*, Size and morphology of the Chicxulub impact crater. *Nature* **390**, 472-476 (1997).
5. P. Schulte *et al.*, The Chicxulub Asteroid Impact and Mass Extinction at the Cretaceous-Paleogene Boundary. *Science* **327**, 1214-1218 (2010).
6. G. Ravizza, D. VonderHaar, A geochemical clock in earliest Paleogene pelagic carbonates based on the impact-induced Os isotope excursion at the Cretaceous-Paleogene boundary. *Paleoceanography* **27**, PA3219 (2012).
7. F. M. Gradstein, J. G. Ogg, M. D. Schmitz, G. M. Ogg, *The Geologic Time Scale 2012*. (Elsevier B.V., Amsterdam, 2012).
8. B. Schoene *et al.*, U-Pb constraints on pulsed eruption of the Deccan Traps across the end-Cretaceous mass extinction. *Science* **363**, 862-866 (2019).
9. C. J. Sprain *et al.*, The eruptive tempo of Deccan volcanism in relation to the Cretaceous-Paleogene boundary. *Science* **363**, 866-870 (2019).
10. A. L. Chenet *et al.*, Determination of rapid Deccan eruptions across the Cretaceous-Tertiary boundary using paleomagnetic secular variation: 2. Constraints from analysis of eight new sections and synthesis for a 3500-m-thick composite section. *Journal of Geophysical Research-Solid Earth* **114**, B06103 (2009).
11. A. L. Chenet, X. Quidelleur, F. Fluteau, V. Courtillot, S. Bajpai, K-40-Ar-40 dating of the Main Deccan large igneous province: Further evidence of KTB age and short duration. *Earth and Planetary Science Letters* **263**, 1-15 (2007).
12. B. Schoene *et al.*, U-Pb geochronology of the Deccan Traps and relation to the end-Cretaceous mass extinction. *Science* **347**, 182-184 (2015).
13. P. R. Renne *et al.*, State shift in Deccan volcanism at the Cretaceous-Paleogene boundary, possibly induced by impact. *Science* **350**, 76-78 (2015).
14. P. R. Renne *et al.*, Time Scales of Critical Events Around the Cretaceous-Paleogene Boundary. *Science* **339**, 684-687 (2013).
15. M. A. Richards *et al.*, Triggering of the largest Deccan eruptions by the Chicxulub impact. *Geological Society of America Bulletin* **127**, 1507-1520 (2015).
16. E. Font *et al.*, Deccan volcanism induced high-stress environment during the Cretaceous-Paleogene transition at Zumaia, Spain: Evidence from magnetic, mineralogical and biostratigraphic records. *Earth and Planetary Science Letters* **484**, 53-66 (2018).
17. N. Artemieva, J. Morgan, E. S. Party, Quantifying the Release of Climate-Active Gases by Large Meteorite Impacts With a Case Study of Chicxulub. *Geophysical Research Letters* **44**, 10180-10188 (2017).
18. S. P. S. Gulick *et al.*, The first day of the Cenozoic. *Proceedings of the National Academy of Sciences of the United States of America* **116**, 19342-19351 (2019).

19. D. A. Kring, D. D. Durda, Trajectories and distribution of material ejected from the Chicxulub impact crater: implications for postimpact wildfires. *Journal of Geophysical Research-Planets* **107**, (2002).
20. J. Morgan, N. Artemieva, T. Goldin, Revisiting wildfires at the K-Pg boundary. *J Geophys Res-Biogeo* **118**, 1508-1520 (2013).
21. S. Ohno *et al.*, Production of sulphate-rich vapour during the Chicxulub impact and implications for ocean acidification. *Nature Geoscience* **7**, 279-282 (2014).
22. T. Tyrrell, A. Merico, D. I. A. McKay, Severity of ocean acidification following the end-Cretaceous asteroid impact. *Proceedings of the National Academy of Sciences of the United States of America* **112**, 6556-6561 (2015).
23. M. J. Henehan *et al.*, Rapid ocean acidification and protracted Earth System recovery followed the end-Cretaceous Chixulub impact. *Proceedings of the National Academy of Sciences of the United States of America*, (2019).
24. J. Vellekoop *et al.*, Rapid short-term cooling following the Chicxulub impact at the Cretaceous-Paleogene boundary. *Proceedings of the National Academy of Sciences of the United States of America* **111**, 7537-7541 (2014).
25. K. Kaiho *et al.*, Global climate change driven by soot at the K-Pg boundary as the cause of the mass extinction. *Sci Rep-Uk* **6**, (2016).
26. J. Brugger, G. Feulner, S. Petri, Baby, it's cold outside: Climate model simulations of the effects of the asteroid impact at the end of the Cretaceous. *Geophysical Research Letters* **44**, 419-427 (2017).
27. C. G. Bardeen, R. R. Garcia, O. B. Toon, A. J. Conley, On transient climate change at the Cretaceous-Paleogene boundary due to atmospheric soot injections. *Proceedings of the National Academy of Sciences of the United States of America* **114**, E7415-E7424 (2017).
28. L. Alegret, E. Thomas, K. C. Lohmann, End-Cretaceous marine mass extinction not caused by productivity collapse. *Proceedings of the National Academy of Sciences of the United States of America* **109**, 728-732 (2012).
29. B. J. Marshall, R. C. Thunell, M. J. Henehan, Y. Astor, K. E. Wejnert, Planktonic foraminiferal area density as a proxy for carbonate ion concentration: A calibration study using the Cariaco Basin ocean time series. *Paleoceanography* **28**, 363-376 (2013).
30. M. Aberhan, S. Weidemeyer, W. Kiessling, R. A. Scasso, F. A. Medina, Faunal evidence for reduced productivity and uncoordinated recovery in Southern Hemisphere Cretaceous-Paleogene boundary sections. *Geology* **35**, 227-230 (2007).
31. P. M. Sheehan, T. A. Hansen, Detritus Feeding as a Buffer to Extinction at the End of the Cretaceous. *Geology* **14**, 868-870 (1986).
32. D. S. Robertson, M. C. McKenna, O. B. Toon, S. Hope, J. A. Lillegraven, Survival in the first hours of the Cenozoic. *Geological Society of America Bulletin* **116**, 760-768 (2004).
33. E. M. Shoemaker, Impact cratering through geologic time. *Journal of the Royal Astronomical Society of Canada* **92**, 297-309 (1998).
34. J. D. Archibald *et al.*, Cretaceous Extinctions: Multiple Causes. *Science* **328**, 973-973 (2010).
35. G. Keller, J. Punekar, P. Mateo, Upheavals during the Late Maastrichtian: Volcanism, climate and faunal events preceding the end-Cretaceous mass extinction. *Palaeogeography Palaeoclimatology Palaeoecology* **441**, 137-151 (2016).
36. S. V. Sobolev *et al.*, Linking mantle plumes, large igneous provinces and environmental catastrophes. *Nature* **477**, 312-U380 (2011).

37. M. T. Jones, D. A. Jerram, H. H. Svensen, C. Grove, The effects of large igneous provinces on the global carbon and sulphur cycles. *Palaeogeography Palaeoclimatology Palaeoecology* **441**, 4-21 (2016).
38. A. Schmidt *et al.*, Selective environmental stress from sulphur emitted by continental flood basalt eruptions. *Nature Geoscience* **9**, 77-82 (2016).
39. S. Self, S. Blake, K. Sharma, M. Widdowson, S. Sephton, Sulfur and chlorine in Late Cretaceous Deccan magmas and eruptive gas release. *Science* **319**, 1654-1657 (2008).
40. Materials and methods are available as supplementary materials at the Science website.
41. M. J. Henehan, P. M. Hull, D. E. Penman, J. W. B. Rae, D. N. Schmidt, Biogeochemical significance of pelagic ecosystem function: an end-Cretaceous case study. *Philosophical Transactions of the Royal Society B-Biological Sciences* **371**, 20150510 (2016).
42. J. S. K. Barnet *et al.*, A new high-resolution chronology for the late Maastrichtian warming event: Establishing robust temporal links with the onset of Deccan volcanism. *Geology* **46**, 147-150 (2018).
43. J. S. K. Barnet *et al.*, A high-fidelity benthic stable isotope record of Late Cretaceous-Early Eocene climate change and carbon-cycling. *Paleoceanography and Paleoclimatology* **34**, 672-691 (2019).
44. L. Q. Li, G. Keller, Abrupt deep-sea warming at the end of the Cretaceous. *Geology* **26**, 995-998 (1998).
45. R. D. Norris, P. A. Wilson, P. Blum, a. t. E. Scientists, in *Proc. IODP, 342,* R. D. Norris, Wilson, P.A., Blum, P., and the Expedition 342 Scientists, Ed. (Integrated Ocean Drilling Program, College Station, TX, 2014).
46. N. Robinson, G. Ravizza, R. Coccioni, B. Peucker-Ehrenbrink, R. Norris, A high-resolution marine Os-187/Os-188 record for the late Maastrichtian: distinguishing the chemical fingerprints of Deccan volcanism and the KP impact event. *Earth and Planetary Science Letters* **281**, 159-168 (2009).
47. R. E. Zeebe, LOSCAR: Long-term Ocean-atmosphere-Sediment CArbon cycle Reservoir Model v2.0.4. *Geoscientific Model Development* **5**, 149-166 (2012).
48. J. C. Zachos, M. A. Arthur, W. E. Dean, Geochemical evidence for suppression of pelagic marine productivity at the Cretaceous/Tertiary boundary. *Nature* **337**, 61-64 (1989).
49. H. S. Birch, H. K. Coxall , P. N. Pearson, D. Kroon, D. N. Schmidt, Partial collapse of the marine carbon pump after the Cretaceous-Paleogene boundary. *Geology* **44**, 287-290 (2016).
50. C. J. Sprain, P. R. Renne, W. A. Clemens, G. P. Wilson, Calibration of chron C29r: New high-precision geochronologic and paleomagnetic constraints from the Hell Creek region, Montana. *Geological Society of America Bulletin* **130**, 1615-1644 (2018).
51. E. J. Rohling *et al.*, Comparing Climate Sensitivity, Past and Present. *Annual Review of Marine Science, Vol 10* **10**, 261-+ (2018).
52. K. G. MacLeod, P. C. Quinton, J. Sepulveda, M. H. Negra, Postimpact earliest Paleogene warming shown by fish debris oxygen isotopes (El Kef, Tunisia). *Science* **360**, 1467-1469 (2018).
53. S. D'Hondt, P. Donaghay, J. C. Zachos, D. Luttenberg, M. Lindinger, Organic carbon fluxes and ecological recovery from the Cretaceous-Tertiary mass extinction. *Science* **282**, 276-279 (1998).

54. J. D. Witts *et al.*, Macrofossil evidence for a rapid and severe Cretaceous-Paleogene mass extinction in Antarctica. *Nat Commun* **7**, 11738 (2016).
55. T. S. Tobin, Recognition of a likely two phased extinction at the K-Pg boundary in Antarctica. *Sci Rep-Uk* **7**, 16317 (2017).
56. P. M. Hull, R. D. Norris, T. J. Bralower, J. D. Schueth, A role for chance in marine recovery from the end-Cretaceous extinction. *Nature Geoscience* **4**, 856-860 (2011).
57. J. J. Pospichal, in *The Cretaceous-Tertiary event and other catastrophes in Earth history: Geological Society of America Special Paper 307,* G. Ryder, D. Fastovsky, S. Gartner, Eds. (1996), pp. 335-360.
58. E. C. Sibert, M. Friedman, P. M. Hull, G. Hunt, R. D. Norris, Two pulses of origination in Pacific pelagic fish following the Cretaceous-Paleogene Mass Extinction. *Proceedings of the Royal Society B-Biological Sciences*, 20181194 (2018).
59. M. Edmonds, New geochemical insights into volcanic degassing. *Philosophical Transactions of the Royal Society a-Mathematical Physical and Engineering Sciences* **366**, 4559-4579 (2008).
60. P. F. Sexton *et al.*, Eocene global warming events driven by ventilation of oceanic dissolved organic carbon. *Nature* **471**, 349-352 (2011).
61. R. D. Norris, in *Palaeobiology II,* D. E. G. Briggs, P. G. Crowther, Eds. (Blackwell Science Ltd., Oxford, 2001), pp. 229-231.

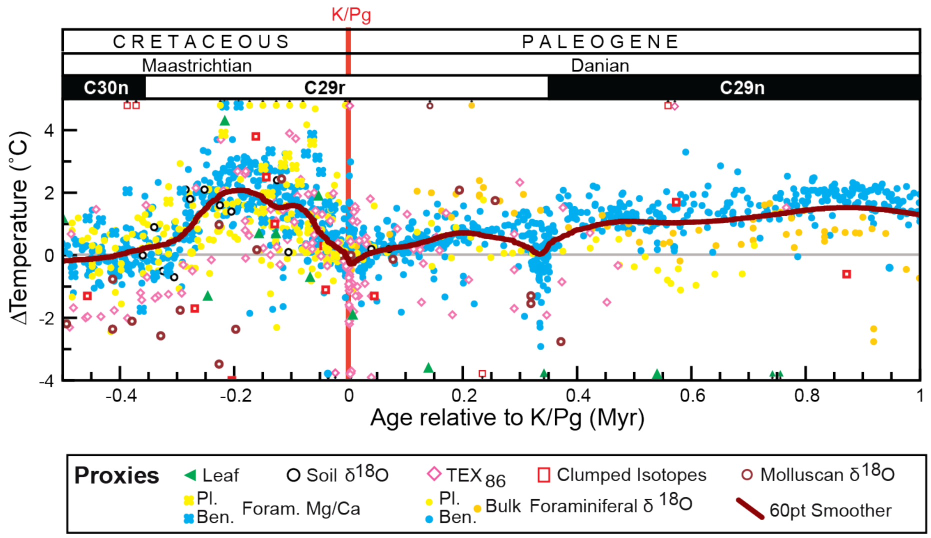

Figure 1. Global temperature change across the Cretaceous-Paleogene boundary. New and existing empirical temperature records from marine sediments (foraminiferal $\delta^{18}O$ and Mg/Ca, TEX_{86}), shallow marine carbonates (clumped isotopes of mollusk carbonate), and terrestrial proxies (leaf margin analysis, biomarkers, clumped isotopes of mollusk carbonate) were aligned to common age model (Table S2 and S3) and normalized to the latest Cretaceous temperature within each record. A 60pt fast Fourier transform smoother of global temperature change is shown in dark red. Data are provided in Table S4-S12. Some outlying data points do not fall within plot bounds, but can be seen in Figs. S1-S16.

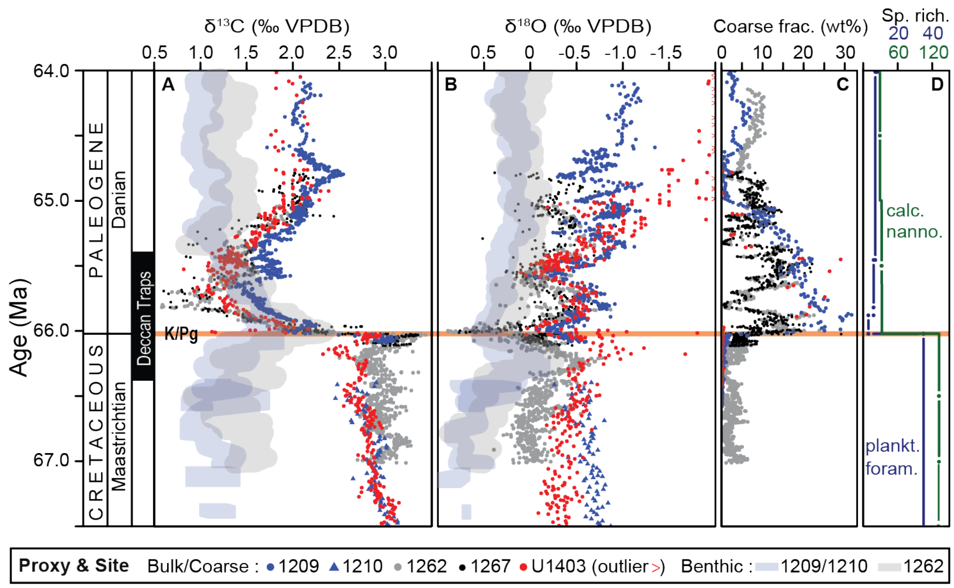

Figure 2. K/Pg boundary dynamics at the best-resolved deep-sea sites globally: Shatsky Rise, Walvis Ridge, and J-Anomaly Ridge. High resolution carbon (A) and oxygen (B) isotope dynamics in benthic foraminifera (transparent lines) and bulk carbonate (discrete points), and sediment composition (C, weight % coarse fraction), at Shatsky Rise (blue), Walvis Ridge (grey), and J-Anomaly Ridge (red), compared to (D) global records of nannofossil (grey) and foraminifera (blue, from (*61*)) species richness (*40*). Major interval of Deccan Trap emplacement (estimated 93% of volume) indicated at left by the black bar, after ref 9.

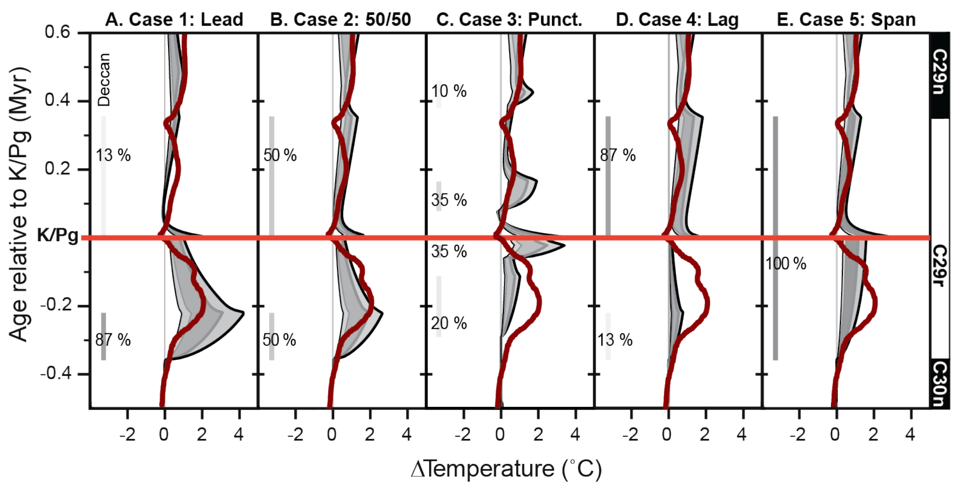

Figure 3. Global temperature change across the Cretaceous-Paleogene boundary as compared to five scenarios for Deccan Trap outgassing. Outgassing scenarios include (A) Case 1 (Leading): most outgassing prior to impact, (B) Case 2 (50/50): 50% outgassing prior to and 50% post impact, (C) Case 3 (Punctuated), (D) Case 4 (Lagging): most outgassing post impact, and (E) Case 5 (Spanning): continuous outgassing throughout magnetochron C29r (Table 1). Each model scenario is represented by four lines (bounding a shaded region) delineating different combinations of climate sensitivity and volcanic outgassing: high degassing (9545 GtC and 8500 GtS) and 3°C/doubling (thick grey line); high degassing and 4°C/doubling (thick black line); low degassing (4090 GtC and 3200 GtS) and 3°C/doubling (thin grey line), and low degassing and 2°C/doubling (thin black line), and compared to a 60pt fast Fourier transform smoother of global temperature change (red line) from Fig. 1. Deccan outgassing timing indicated by bars at left, with the shading intensity of the bar indicative of the proportion outgassing in that interval.

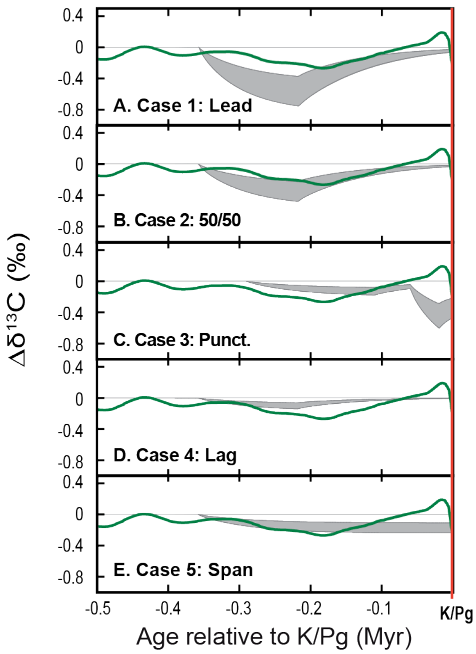

Figure 4. Surface ocean $\delta^{13}C$ change across the late Maastrichtian warming as compared to five scenarios for Deccan Trap outgassing. Bulk carbonate $\Delta\delta^{13}C$ (20pt fast Fourier transform smoother of Site U1403 and Site 1262 data) shown against surface ocean $\delta^{13}C$ for end-member outgassing and climate sensitivity scenarios (grey envelope) for each case as detailed in Fig. 3. In each case, carbonate carbon isotopes are expressed as $\Delta\delta^{13}C$, relative to the late Maastrichtian high of 3.03 ‰ at 0.432 Myr prior to the onset of the CO_2 release (see also Figs. S36-S37).

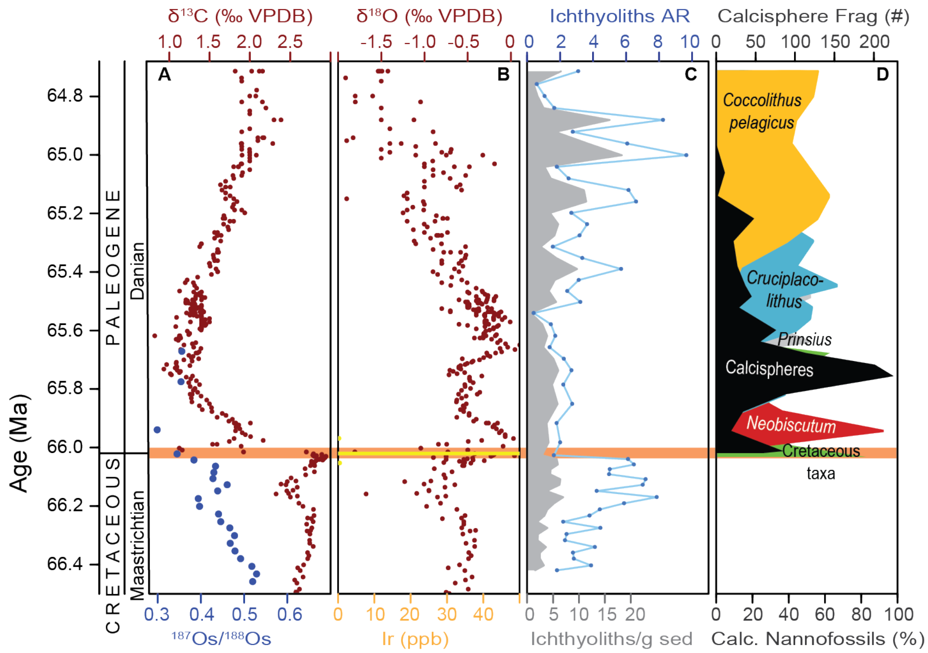

Figure 5. Late Cretaceous warming and early Paleocene record of environmental and biotic change at IODP Site U1403, J-Anomaly Ridge, Newfoundland. A negative carbon isotope anomaly (A) coincides with late Cretaceous warming in $\delta^{18}O$ (B), and osmium isotope evidence for volcanism (A) at IODP Site U1403. The collapse in surface ocean $\delta^{13}C$ values (A) coincides with iridium anomaly (B), and step change in fish tooth accumulation (C). Earliest Paleocene $\delta^{18}O$ values of bulk carbonate appear to be strongly influenced by vital effects driven by rapid turnover in the dominant calcareous nannofossil taxa (D) in sites globally (Figs. S18, S34, S35). Data in Tables S12, S16, S17, S29.

Table 1. Model parameters for five focal Deccan outgassing scenarios tested in LOSCAR.

		Case 1: Leading	Case 2: 50/50	Case 3: Punct.	Case 4: Lagging	Case 5: Spanning
Volcanic Outgassing	*Pulse 1 (Pre): Volume*	87% of total h: 8305 Gt C, 7395 Gt S l: 3559 Gt C, 2784 Gt S	50% of total high: 4773 Gt C, 4250 Gt S low: 2045 Gt C, 1600 Gt S	20% of total h: 1909 Gt C, 1700 Gt S l: 818 Gt C, 640 Gt S	13% of total high: 1241 Gt C, 1105 Gt S low: 532 Gt C, 416 Gt S	100% of total high: 9545 Gt C, 8500 Gt S low: 4091 Gt C, 3200 Gt S
	Timing	Starts: -358 kyr Ends: -218 kyr	Starts: -358 kyr Ends: -218 kyr	Starts: -290 kyr Ends: -110 kyr	Starts: -358 kyr Ends: -218 kyr	Starts: -358 kyr Ends: 355 kyr
	Pulse 2 (Pre): Volume			35% of total h: 3340 Gt C, 2975 Gt S l: 1431 Gt C, 1120 Gt S		
	Timing			Starts: -60 kyr Ends: -20 kyr		
	Pulse 1 (Post): Volume	13% of total h: 1241 Gt C, 1105 Gt S l: 532 Gt C, 416 Gt S	50% of total high: 4773 Gt C, 4250 Gt S low: 2045 Gt C, 1600 Gt S	35% of total h: 3340 Gt C, 2975 Gt S l: 1431 Gt C, 1120 Gt S	87% of total high: 8305 Gt C, 7395 Gt S low: 3559 Gt C, 2784 Gt S	
	Timing	Starts: 0 kyr Ends: 355 kyr	Starts: 0 kyr Ends: 355 kyr	Starts: 80 kyr Ends: 170 kyr	Starts: 0 kyr Ends: 355 kyr	
	Pulse 2 (Post): Volume			10% of total h: 955 Gt C, 850 Gt S l: 409 Gt C, 320 Gt S		
	Timing			Starts: 390 kyr Ends: 430 kyr		
Impact Outgas.	*Volume*	100% of total 115 Gt C, 325 Gt S	100% of total 115 Gt C, 325 Gt S	100% of total 115 Gt C, 325 Gt S	100% of total 115 Gt C, 325 Gt S	100% of total 115 Gt C, 325 Gt S
	Timing	Starts: 0 kyr Ends: 1 kyr	Starts: 0 kyr Ends: 1 kyr	Starts: 0 kyr Ends: 1 kyr	Starts: 0 kyr Ends: 1 kyr	Starts: 0 kyr Ends: 1 kyr
Biotic Change	*Organic Export Flux Δ*	50% reduction	50% reduction	50% reduction	50% reduction	50% reduction
	$CaCO_3$ Export Flux Δ	42.5% reduction	42.5% reduction	42.5% reduction	42.5% reduction	42.5% reduction
	Frac. Int.-depth C_{org} remin. Δ	22% increase	22% increase	22% increase	22% increase	22% increase
	Timing	Starts: 0 kyr immediately tapers Ends: 1770 kyr	Starts: 0 kyr immediately tapers Ends: 1770 kyr	Starts: 0 kyr immediately tapers Ends: 1770 kyr	Starts: 0 kyr immediately tapers Ends: 1770 kyr	Starts: 0 kyr immediately tapers Ends: 1770 kyr

Table 2. Mean absolute error (MAE) and mean minimum absolute error (MMAE) of cases relative to the interpolated global temperature record. The mean minimum absolute error (MMAE) was calculated for each case by determining whether the empirical data fell outside of the temperature range bounded by the high and low outgassing scenarios given a climate sensitivity of 3°C/CO_2 doubling, and, if so, by how much. MAEs were also calculated for each outgassing volume and climate sensitivity shown in Fig. 3. MMAEs and MAEs were calculated on a 20 kyr interpolated time step from 360kyr prior to 600 kyr post K/Pg. Case 2 consistently has the lowest MAEs and Case 1 and 2 have the lowest MMAEs.

	Mean Min. Abs. Error	***High Volc., 3°C/CO_2 doub.***	***High Volc., 4°C/CO_2 doub.***	***Low Volc., 3°C/CO_2 doub***	***Low Volc., 2°C/CO_2 doub***
Case 1	0.25	0.46	0.65	0.50	0.58
Case 2	0.21	0.35	0.43	0.48	0.58
Case 3	0.45	0.59	0.65	0.58	0.64
Case 4	0.45	0.61	0.69	0.56	0.63
Case 5	0.29	0.40	0.44	0.53	0.61